Available online at www.sciencedirect.com
SCIENCE DIRECT®
Journal of Computational Physics 187 (2003) 492–503
JOURNAL OF COMPUTATIONAL PHYSICS
www.elsevier.com/locate/jcp

Boundary-integral simulations of containerless solidification

Vladimir S. Ajaev *, Stephen H. Davis

Department of Mathematics, Southern Methodist University, Dallas, TX 75275, USA
Department of Engineering Sciences and Applied Mathematics, Northwestern University, Evanston, IL 60208, USA

Received 25 March 2002; received in revised form 9 November 2002; accepted 28 January 2003

Abstract

We carry out boundary-integral simulations of a two-dimensional liquid droplet surrounded by air and solidified from a cool point on the boundary. There are three interfaces in the problem: solid–liquid, air–liquid, and air–solid. All three evolve in time in such a way that certain tri-junction conditions must be satisfied. Our numerical method describes the quasi-steady evolution of the interfaces in the limit of zero surface energy on the solidification front. A new iterative technique is developed to describe the interface evolution when mass and total energy are conserved and the local tri-junction conditions are satisfied at every instant in time. A method is also developed for efficient numerical integration over the interfaces by taking advantage of analytical formulas for Green's functions. We start the simulations by studying the case of equal densities of the solid and liquid. This allows us to verify the numerical method and obtain some estimates of the speed of the solidification front. Solid–liquid interface flattening is observed at the intermediate stages of solidification. When the densities of the two phases are different, elongated solidified particles are observed when the solid density is smaller than the liquid density. At the final stages of solidification, a corner is formed in agreement with observations in related experiments.

Keywords: Boundary-integral method; Droplet solidification; Contact lines

1. Introduction

Containerless solidification is important for many technological processes. In particular, the rapid cooling of clouds of small liquid droplets is often used for production of powders. Sprays of molten liquid droplets exit a nozzle and come into contact with cold air, solidify, and then fall to the substrate. Experimental observations [1,2] show that the solidification front originates from a small nucleus of solid phase on a boundary and the shapes of the interface and the droplet change as the front propagates through the droplet.

In order to model this process mathematically one has to impose proper boundary conditions at the tri-junctions, the regions where solid, liquid, and air meet; we also refer to these as contact lines. Contact-line

* Corresponding author. Tel.: +1-214-768-3629; fax: +1-214-768-2355.
E-mail address: ajaev@mail.smu.edu (V.S. Ajaev).

0021-9991/03/$ - see front matter
doi:10.1016/S0021-9991(03)00120-7

phenomena have been studied extensively in fluid mechanics [3,4]. However, apart from the use of Young's equation (a condition of thermodynamic equilibrium), there is very little theoretical work on the topic in the context of materials science in *dynamical* situations. This is despite the fact that the importance of contact-line conditions in solidification has been recognized in the literature [5,6]. Anderson et al. [7] froze sessile water drops and found that the solidified drop possesses a cusp at its apex. A rough analysis suggested that a non-equilibrium boundary condition at the tri-junction must be posed in order to describe evolution of the solidification front in a freezing drop. Ajaev and Davis [8] considered directional solidification of a binary alloy in Hele–Shaw cell, for both fixed and velocity-dependent angles between the solid–liquid interface and the sidewall, and showed that the contact-line conditions influence both the stability and nonlinear evolution of the solidification front.

In order to develop a realistic model for droplet solidification, local contact-line conditions have to be incorporated into a robust numerical scheme for evolution of the shapes of domains of solid and liquid phases. Several numerical methods have been used for studies of moving-boundary problems in solidification. Finite-difference approach with an elaborate interface-tracking algorithm has been used for simulations of dendritic solidification [9]. Finite-element methods have been used to study solidification of droplets by Fukai et al. [10]. They consider deformation of a liquid droplet that comes into contact with cold substrate and solidifies. A triangular finite-element grid is used for simulations. The grid evolves in time to maintain the accuracy of the solution in the deforming domain. Clearly, the presence of moving boundaries makes applying the standard finite-difference and finite-element approaches less straightforward than for boundary-value problems on fixed domains. Therefore alternative approaches have been considered in the literature. Phase-field methods treat interfaces as regions of rapid changes in an auxiliary order parameter, or phase field [11]. The phase field takes two different constant values in the bulks of the two phases. Simulation then involves evolution of the phase field as opposed to the tracking of a free boundary. Level-set methods have been successfully used for simulations of solidifying interfaces [12]. In this approach the solid–liquid interface is represented as a zero contour of a level-set function. Solving an equation for this function implicitly describes the motion of the interface. Finally, boundary-element type methods have been used for problems with phase change [13]. A more detailed discussion of different methods for simulations of moving boundaries can be found in several review articles [14–16].

The problem considered in the present study is characterized by the presence of tri-junctions. Relatively few numerical methods for solidification have been extended to include the effect of tri-junctions. In [17] the motion of tri-junctions was simulated using level-set methods with the local velocities of several interfaces determining the motion; no contact-line condition dictated by the physics was imposed. Jacqmin [18] investigated how phase-field methods can be used for simulations of moving contact lines in fluid mechanics. An elaborate combination of asymptotic and numerical methods in the vicinity of the contact line allowed him to model simple wetting and dewetting flows.

We choose the boundary-integral method (cf. Kythe [19]) for our studies of droplet solidification. A boundary-integral method has been recently suggested for solidification of droplets on a substrate [20]. It has advantages of reducing the dimension of the problem as well as leading to a relatively straightforward implementation of the contact-line conditions. We generalize the ideas of the boundary-integral method to solidification in domains with time-dependent boundaries and contact-line conditions. The problem formulation is motivated by experiments on rapid freezing of small droplets, although the agreement with experimental results can only be qualitative since we consider quasi-steady two-dimensional evolution here in a model that ignores the non-equilibrium effects at the solid–liquid interface required to describe rapid solidification. Generally, both the solid–liquid interface and the boundary between droplet and outside air change in time, so both have to be determined as part of the numerical solution. We consider evolution of solid–liquid interface and final shapes of solidified particles for different values of the density ratios of the two phases in the limit of zero surface tension on the solid–liquid interface.

The paper is organized as follows. In Section 2 we formulate the physical problem of interest and define several important non-dimensional parameters. In Section 3 various aspects of the numerical method are explained. We re-formulate the problem in terms of integral equations, then discuss efficient methods for solving these equations, as well as methods for describing time-evolution of interfaces. In Section 4 we discuss some physical results obtained from our numerical simulations. Finally, in Section 5 we summarize both numerical method and important physical results.

2. Formulation

We consider propagation of a solidification front in a liquid droplet cooled locally at a point on the surface, P. The regions of solid and liquid phases are denoted by Ω_S and Ω_L, respectively; they are shown schematically in Fig. 1. Heat conduction in both phases is described by Laplace's equations:

$$\nabla^2 T = 0 \quad \text{in } \Omega_L, \tag{1}$$

$$\nabla^2 T' = 0 \quad \text{in } \Omega_S. \tag{2}$$

Here T and T' are temperature fields in liquid and solid phases, respectively, scaled by the melting temperature, T_m. We choose the initial radius of the droplet, R, as the length scale. The quasi-steady approximation used implies that transients in full (unsteady) heat conduction problem decay much faster than the front advances.

In the absence of surface tension the temperature T^i at the solid–liquid interface is the equilibrium melting temperature, T_m, so the non-dimensional temperature boundary condition at the solid–liquid interface is

$$T^i = 1. \tag{3}$$

Although we concentrate on formulating the numerical method for the simplified case of negligible surface tension at the solid–liquid interface, our method can be easily extended to include it. The effects of the non-zero surface energy will be investigated in subsequent publications.

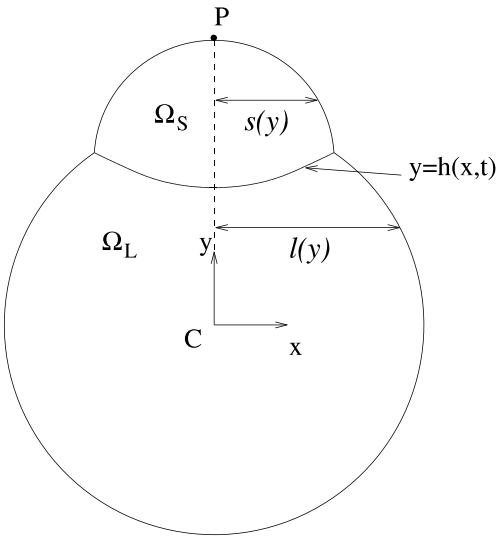

Fig. 1. Configuration of solidifying droplet cooled at a point. The solidification front separates regions of solid, Ω_S, and liquid, Ω_L, phases. Cartesian coordinates (x, y) are also shown.

The heat-flux condition at the solidifying interface is written in the form

$$V_n = \frac{\partial T'}{\partial n} - k_T \frac{\partial T}{\partial n}, \tag{4}$$

where $k_T = k_L/k_S$, k_S and k_L are the thermal conductivities of solid and liquid, respectively, and $\partial/\partial n$ denotes normal derivative. The velocity is scaled by $U = k_S T_m/R\mathscr{L}\rho_S$, where $\mathscr{L}$ is the latent heat, ρ_S is the density of the solid phase; time is scaled by R/U. In addition to the general conditions (3) and (4), the contact-line conditions and initial data are specified depending on geometry.

Let us now apply the above general model to the *two-dimensional* droplet, which is initially centered at a point C. We choose non-dimensional Cartesian coordinates (x, y) with the origin at the point C such that the y-axis is along the line CP and assume that the position of the solidification front is described by a function $y = h(x, t)$. The outer boundaries of the liquid region, Ω_L, and solid region, Ω_S, are described by the distances to the y-axis, $l(y, t)$ and $s(y, t)$, respectively, as shown in Fig. 1. We introduce these functions to simplify problem formulation; the numerical method does not require s and l to be single-valued functions of y.

Since air is a relatively poor heat conductor, we apply a no-flux condition everywhere on the outer surfaces except near the point P where the flux is large. It is written in the following non-dimensional form:

$$\frac{\partial T'}{\partial n} = -\frac{q_0}{a\sqrt{\pi}} e^{-(\xi-\xi_P)^2/a^2}, \tag{5}$$

where q_0 is the total flux, ξ is the arc-length variable along the boundary, ξ_P corresponds to the point P; the characteristic size a of the region where the surface is cooled, is small. This simplified model of localized cooling is chosen here to illustrate the numerical method. Any boundary conditions for heat flux motivated by experiments can be used in the framework of our method, even if cooling is not so highly localized.

At the tri-junction between the solid, liquid, and air the contact angle is specified:

$$\phi_S = \frac{\pi}{2} + \tan^{-1} h_x + \tan^{-1} s_y,$$

$$\phi_L = \frac{\pi}{2} - \tan^{-1} h_x - \tan^{-1} l_y,$$

where ϕ_S and ϕ_L are fixed contact angles in the solid and liquid phases. The total mass is conserved during the phase transition, which gives

$$\rho V_S + V_L = \text{const.},$$

where $\rho = \rho_S/\rho_L$ is the density ratio of the two phases, and V_S and V_L are their volumes scaled by the initial volume.

Finally, the initial conditions have to be specified. We assume that the solid–liquid interface initially has constant curvature, the domain of solid phase is small compared to the liquid phase, and the outer boundaries of both domains have constant curvature.

3. Boundary-integral method

3.1. Integral equations

We use boundary-integral method [19] to solve the two-dimensional problem formulated in the previous section. In this and the following subsection we discuss quasi-steady heat conduction in the two phases;

evolution of the interface in time will be considered in Sections 3.3 and 3.4. Thus, we start by discussing the numerical solution of Laplace's equation for the domains with fixed boundaries, Ω_S and Ω_L. First, consider the domain of the solid phase, Ω_S. Instead of solving the Laplace's equation in the bulk of material we reduce the problem to an integral equation for the points on the boundary by using standard Green's-function technique [19]. The value of temperature at a point on the boundary of the domain of solid phase is expressed in terms of the integral over the boundary of Ω_S according to

$$\int_{\partial\Omega_S} (G_0\mathbf{n}\cdot\nabla T' - T'\mathbf{n}\cdot\nabla G_0)\,\mathrm{d}\xi = \frac{1}{2}T', \tag{6}$$

where $\mathbf{n}$ is the unit outward normal to the region Ω_S, $\mathrm{d}\xi = \sqrt{\mathrm{d}x^2 + \mathrm{d}y^2}$ is the length element along the boundary, G_0 is the free-space Green's function,

$$G_0 = -\frac{1}{4\pi}\ln[(x-x')^2 + (y-y')^2]. \tag{7}$$

The integral on the left-hand side of Eq. (6) is over the boundary of the domain Ω_S, which consists of the solid–liqud and solid–air interfaces, denoted by I_{sl} and I_{sa}, respectively. The integral over the solid–air interface can be written in a different form using the condition for heat flux (5):

$$\int_{I_{sa}} (G_0\mathbf{n}\cdot\nabla T' - T'\mathbf{n}\cdot\nabla G_0)\,\mathrm{d}\xi = \frac{q_0}{a\sqrt{\pi}}\int_{I_{sa}} G_0 \mathrm{e}^{-(\xi-\xi_P)^2/a^2}\,\mathrm{d}\xi - \int_{I_{sa}} T'\mathbf{n}\cdot\nabla G_0\,\mathrm{d}\xi. \tag{8}$$

We note that in the first term on the right-hand side the integrand decays rapidly away from the point P. After substituting this into the integral equation (6) we obtain

$$\int_{I_{sl}} (G_0\mathbf{n}\cdot\nabla T' - T'\mathbf{n}\cdot\nabla G_0)\,\mathrm{d}\xi + \frac{q_0}{a\sqrt{\pi}}\int_{I_{sa}} G_0 \mathrm{e}^{-(\xi-\xi_P)^2/a^2}\,\mathrm{d}\xi - \int_{I_{sa}} T'\mathbf{n}\cdot\nabla G_0\,\mathrm{d}\xi = \frac{1}{2}T'. \tag{9}$$

A similar approach can be used to describe the heat conduction in the liquid. However, since the surface tension is zero, the temperature of the solid–liquid interface is constant. Together with the no-flux condition at the liquid–air interface this implies that the only solution of the corresponding Laplace's equation is $T = 1$. Thus, the liquid phase in this case has uniform temperature and the flux $\partial T/\partial n$ in (4) is zero. The shape of the liquid domain is then found from the condition of constant curvature and the boundary conditions at the tri-junction where solid, liquid, and air meet, as discussed in Section 3.4. We note, however, that a weak linear dependence of the local front temperature on curvature has to be introduced to achieve convergence in the simulations.

3.2. Numerical evaluation of integrals

In order to solve Eq. (9) one has to discretize the interfaces. We note that the shape of the solidified part of the droplet is in general found from integration in time from some initial conditions (which are discussed in Section 3.3). The solid–liquid interface is parametrized by the normalized arclength variable, α, total length, L, and the angle $\theta(\alpha)$ between the tangent line to the interface and the x-axis [22]. The Cartesian coordinates of an arbitrary point on the interface can be expressed in terms of α as

$$x = \frac{L}{2\pi}\int_0^\alpha \cos\theta\,\mathrm{d}\alpha',$$

$$y = h(0,t) + \frac{L}{2\pi}\int_0^\alpha \sin\theta\,\mathrm{d}\alpha'.$$

Since the interface is symmetric, it is sufficient to consider only the right half, which corresponds to $0 \leqslant \alpha \leqslant \pi$. Numerical integration is performed using fourth-order accurate methods.

After the solid–liquid interface is discretized by dividing the interval $[0, 2\pi]$ into N equal subintervals, evaluating the integral over I_{sl} in Eq. (9) by Gauss–Legendre quadratures with spline interpolation is relatively straightforward. The only difficulty comes from the singularity in G_0 at the source point ($x = x'$, $y = y'$). This singularity can be handled by special choice of weights in integration formulas or removed analytically. We choose the latter approach. Consider integration over a subinterval with the source at one of the end points; the singularity in the integral is removed by means of the following approximation (valid for arbitrary regular function f):

$$\int_0^h f \ln r \, \mathrm{d}r = f(0)h(\ln h - 1),$$

where $h = L/2\pi N$, N is the number of subintervals in the discretization.

The integral equation (9) also requires an integration over the solid–air interface, I_{sa}. Evaluation of the integral of $T'\mathbf{n} \cdot \nabla G_0$ over the solid–liquid interface requires special discussion. We found that use of standard Gauss–Legendre quadratures requires rather large number of grid points to achieve reasonable accuracy. Therefore, a different procedure was developed for numerical integration; it uses some ideas from boundary-integral method for liquid flows [21]. Each segment of solid surface between grid points is represented by a straight line, over which the temperature and heat flux are taken to be constant; their values are the averages of those of the mesh points. An important advantage of using free-space Green's function is the possibility of analytical calculation of the integrals over each element of the interface. Integral over each element can be expressed in terms of positions of the points i and $i + 1$ at the solid–air interface and the position of the singularity, S. If we connect the singularity with the endpoints of the subinterval by the straight lines, as shown in Fig. 2, then the integral over the element can be expressed in terms of angles between these lines and the x-axis:

$$I_i = \frac{T'_i + T'_{i+1}}{4\pi}(\beta^{i+1} - \beta^i). \tag{10}$$

The contributions from each element are added together. This method allows one to find integrals much more efficiently than the standard quadrature formulas.

The resulting discrete system is then solved numerically at all points except corners by a standard Newton–Raphson iteration procedure, which determines $\mathbf{n} \cdot \nabla T'$ and thus the heat flux in the solid phase near the interface.

After the normal components of heat fluxes near the solid–liquid interface are found, their evolution in time can be obtained by substituting their values into the condition for conservation of energy, Eq. (4).

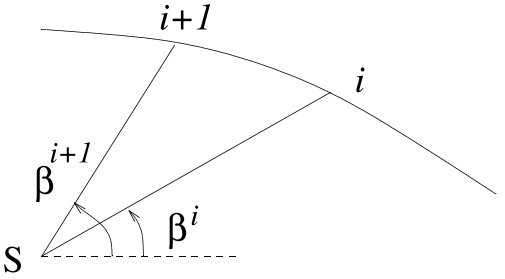

Fig. 2. A sketch for the numerical integration. Integral over the element shown is evaluated analytically using the values of the angles β^i and β^{i+1}, as well as relative position of the singularity S.

3.3. Initial conditions

In order to be able to integrate in time one has to specify the initial conditions. We start with a very small nucleus of solid phase with constant interfacial curvature near the point P on the interface, as shown in Fig. 3. This initial condition is motivated by experimental observations of nucleation of small solid particles at initial stages of solidification. The initial radius of curvature of the solid nucleus, r_0, should be small enough so that the evolution of the interface is not significantly affected by the initial condition. However, the initial nucleus has to be much larger than the region where the interface is cooled to simulate the conditions of cooling at a point. The flux near this point P is distributed according to Gaussian-type function, Eq. (5), which is also illustrated in Fig. 3. The non-dimensional width of that distribution, a, has to be small. We choose $a = r_0/10$ and use the cut-off length of $r_0/2$ for the Gaussian distribution of the flux: q_0 is taken to be identically zero if

$$|\xi - \xi_P| > r_0/2.$$

This simplifies numerical integration in Eq. (9).

We have used the value $r_0 = 0.2$ in our computations below, although we occasionally changed the initial radius to verify that r_0 is sufficiently small to not affect the final shape. Prior to time-stepping we verified convergence of the numerical method for constant-temperature solution ($q_0 = 0$ case) and found that for arbitrary initial condition it takes two or three iterations for the error to decay to 10^{-9}.

3.4. Time-evolution of the interface

In this section we develop the numerical procedure for updating the position of the solid–liquid interface. Several modifications of this procedure were used in calculations depending on the values of the density ratio ρ. We describe in detail only the most general procedure applicable for arbitrary density ratios. As

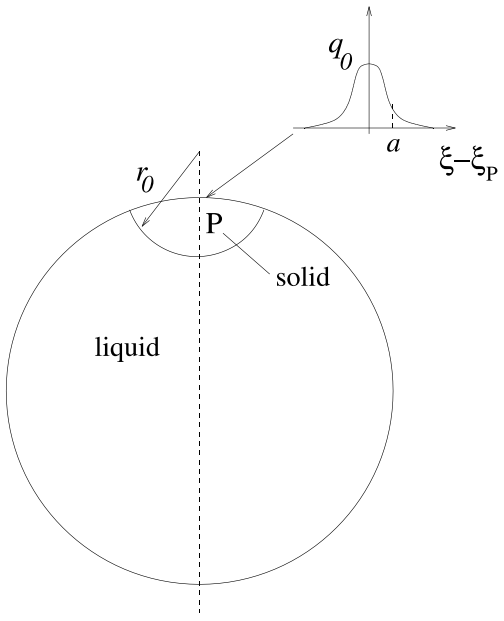

Fig. 3. Initial configuration of the solidifying droplet. A nucleus of the solid phase had constant radius of curvature r_0.

discussed in Section 3.1, the liquid temperature can be taken to be uniform when the surface tension on the solidification front is negligible. We also assume that the liquid–air interface is instantaneously part of a circle of radius R_L.

Let us now discuss how we advance the interfaces in time. First, all points of the solid–liquid interface away from the tri-junctions are advanced according to Eq. (4). This leaves the new length of the interface, L, undetermined, since the new positions of tri-junctions are not yet known. The slope of the air–liquid interface at the tri-junction, ϕ_0, is also an unknown function of time. However, the new positions of the tri-junctions can be expressed as a function of L. The idea is to change L and use local values of $\theta(\alpha)$ to determine the displacement of each interfacial mesh point. Thus, the shapes of both Ω_L and Ω_S at each time step become functions of two variables, L and ϕ_0; two conditions are needed to determine them. The first one comes from conservation of mass; it is written in the form

$$\rho \Delta V_S + \Delta V_L = 0,$$

where the changes in non-dimensional volumes of liquid and solid phases, ΔV_S and ΔV_L, are found by numerical integration over appropriate domains. The second condition is the fixed value of contact angle between the solid–liquid and air–solid interfaces. We note that both conditions are nonlinear, so we need to use an iteration procedure to determine L and ϕ_0 at each time step. A standard Newton–Raphson method tends to put restrictions on time step and occasionally enters non-convergent cycles. We found the Broyden's method [23] to be more efficient. Finally, after each time step is complete, we check whether more points are needed to resolve the air–solid interface properly. If an extra point is inserted between the points of the original grid, the value of temperature at this point is obtained by linear interpolation.

If the densities are equal, then the air–liquid and air–solid interfaces should not change. This provides an important measure of the accuracy of our method: its ability to recover the constant-curvature interface shape, expected to be the only solution for the case of equal densities ($\rho = 1$). We investigated how the numerical value of the radius of curvature depends on the mesh size and time step. A typical plot of the maximum absolute error in finding the radius ($e_R = |R_{num} - 1.0|$) is shown in Fig. 4, where the error is plotted vs. the mesh size h_s for the solid–air interface for fixed time-step $\Delta t = 0.0005$, and $N = 40$. Clearly, the error decays as the number of points is increased. However, it flattens out for small h_s, when errors from discretization of the solid–liquid interface become significant. We also note that convergence is first-order in h_s.

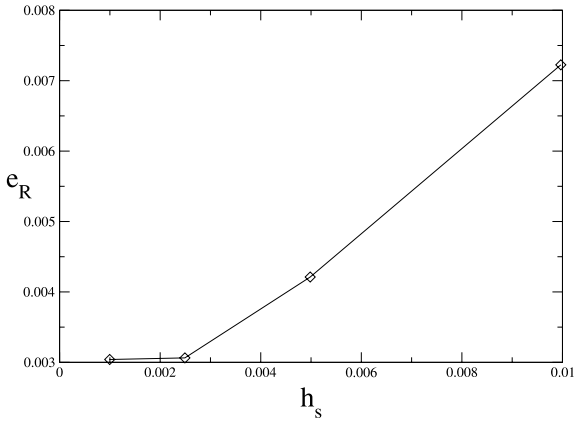

Fig. 4. The maximum absolute error in the radius of the constant-curvature solid–air interface for $\rho = 1$ as a function of the mesh size along the interface. The time step and the number of points in discretization of the solid–liquid interface are fixed ($\Delta t = 0.0005$, $N = 40$).

4. Results and discussion

4.1. Equal densities

Let us first consider the case when the densities of liquid and solid phases are equal, $\rho = 1$, so the front propagation does not lead to deformation of the solid–air and liquid–air interfaces. Evolution of the front for $q_0 = 5.0$, $\phi_S = \phi_L = \pi/2$ is shown in Fig. 5. The front propagates rapidly at the initial stage, but then it slows down and flattens near the middle of the droplet. This behavior is different from that predicted in simplified models where front is concave downward over large periods of time [1].

Since surface tension is absent, the main control parameter is q_0, which measures the degree of local cooling of the droplet. Our simulations show that there are no qualitative changes in the intermediate shapes of the interface when q_0 is varied; though, of course, the solidification occurs faster when q_0 is larger. This is illustrated in Fig. 6, where the average speed of the front is plotted as a function of time for two different values of

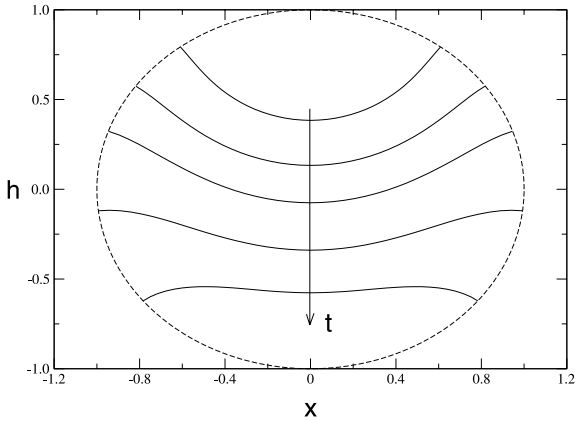

Fig. 5. Evolution of the solid–liquid interface for zero surface tension, $\rho = 1$, and $q_0 = 5.0$. The dashed line denotes the outer boundary of the solidified droplet.

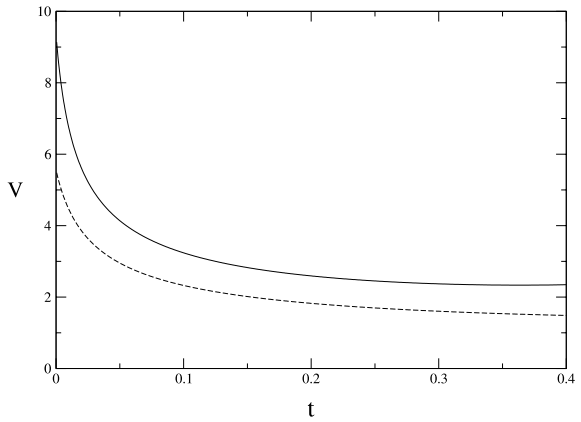

Fig. 6. Average front velocity as a function of time for different values of q_0: $q_0 = 5.0$, solid line, and $q_0 = 3.0$, dashed line.

q_0. We note that in both cases the solidification speed decreases when the interface length L increases, since the amount of heat available for phase change is constant per unit length of the interface in our model.

4.2. Different densities

Numerical results for the case of different densities, $\rho \neq 1$, indicate that the shape of the solidified particle for fixed contact-angle conditions depends on the density ratio. Typical shapes of all three interfaces for $\rho = 0.9$ are shown in Fig. 7 at two consecutive moments in time, $t = 0.05$ and $t = 0.25$. We carry out simulations for $q_0 = 10.0$, $r_0 = 0.2$, $\phi_L = \phi_S = \pi/2$. It is typically sufficient to have not more than 100 mesh points on each interface to obtain accurate solutions. The final shapes of the domain of the solid phase for $\rho = 0.8$ and $\rho = 0.9$ are shown in Fig. 8(a). Larger particles are obtained for smaller ρ, since the mass is conserved. Our simulations also show that the maximum cross-section of the droplet does not change as significantly as the length in the y-direction. Thus, more elongated particles are obtained for

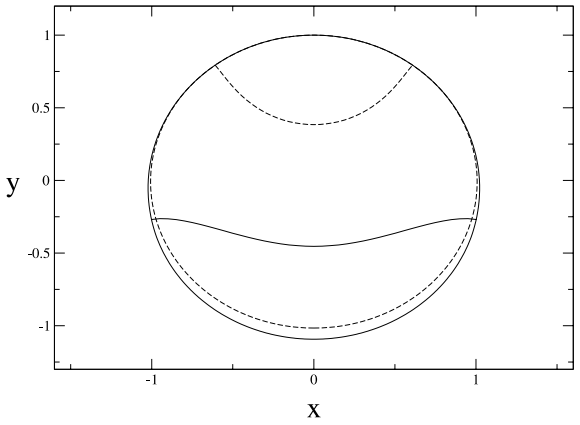

Fig. 7. Intermediate shapes of all three interfaces for $\rho = 0.9$ at two different moments in time: $t = 0.05$ (dashed lines) and $t = 0.25$ (solid lines).

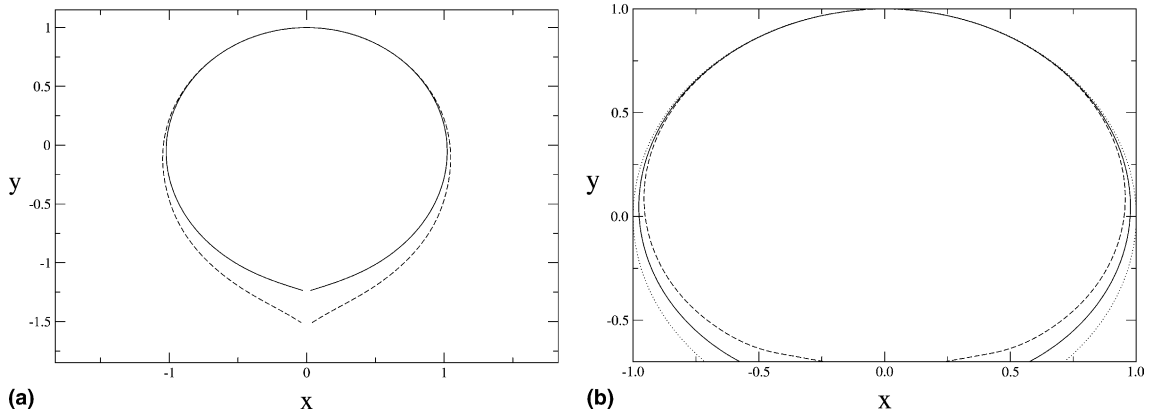

Fig. 8. Shapes of solidifying droplets for various ρ: $\rho = 0.9$, solid line, and $\rho = 0.8$, dashed line in (a); $\rho = 1.1$, solid line, and $\rho = 1.2$, dashed line in (b). Dotted line is $\rho = 1.0$.

smaller values of ρ. We also note that the average velocity of the solidification front decreases as the density ratio is decreased. This also leads to longer solidification times.

We also consider the case when density is larger than 1 and observe similar trends. Typical results for $\rho > 1$ are shown in Fig. 8(b). Smaller particles are obtained in this case.

At the final stages of solidification the curvature of the solid–air interface changes sign, which leads to formation of a corner. This has been observed in experiments on droplet solidification on substrate [7]. The numerical results illustrated in Fig. 8a are consistent with these observations. Numerical results at the final stages of solidification are limited by resolution of the numerical method.

5. Conclusions

We have used the boundary-integral method to simulate droplet solidification. The domains of solid and liquid phases are bounded by three interfaces which are all evolving in time. In the quasi-steady approximation there are two independent tasks in the numerical solution: solving Laplace's equation in domains with fixed boundaries and advancing the boundaries of the domains. The standard Green's function technique allows one to reduce the first task to solving integral equations. An efficient evaluation of the integrals in such integral equation is developed by taking advantage of the properties of free-space Green's function. The second task is to advance the interfaces in time in such a way that both mass and energy are conserved during the phase change. A new procedure is developed that allows one to advance the interface in iterative way to satisfy the conservation conditions, as well as the tri-junction condition at the point where the three phases meet.

Important physical results include the flattening of the interface not predicted by approximate models, as well as corner formation at the final stages of solidification. We have also used the method to study solidification rates and shapes of solidified particles as functions of physical parameters.

Our method has been developed for zero surface tension on the solid–liquid interface, but it can be generalized easily to the case when the surface tension is non-zero. The method can be applied to a variety of interface phase change problems involving tri-junctions.

Acknowledgements

The work was partially supported by the NASA Microgravity Sciences and Applications Program. Professor M.J. Miksis made valuable comments in the process of this work.

References

[1] C.G. Levi, R. Mehrabian, Microstructures of rapidly solidified aluminium alloy submicron powders, Met. Trans. A 13 (1982) 13–23.
[2] C.G. Levi, R. Mehrabian, Heat flow during rapid solidification of undercooled metal droplets, Met. Trans. A 13 (1982) 221–234.
[3] E.B. Dussan V, On the spreading of liquids on solid surfaces: static and dynamic contact lines, Annu. Rev. Fluid Mech. 11 (1979) 371–400.
[4] P.G. De Gennes, Wetting: statics and dynamics, Rev. Mod. Phys. 57 (1985) 827–863.
[5] A. Sanz, The crystallization of a molten sphere, J. Crystal Growth 74 (1986) 642–655.
[6] V.A. Tatarchenko, Survey of quantitative analyses of the effects of capillary shaping on crystal growth, J. Crystal Growth 82 (1987) 74–80.
[7] D.M. Anderson, M.G. Worster, S.H. Davis, The case for a dynamic contact angle in containerless solidification, J. Crystal Growth 168 (1996) 329–338.
[8] V.S. Ajaev, S.H. Davis, Three-dimensional effects in directional solidification in Hele–Shaw cells, Proc. Roy. Soc. A 455 (1999) 3589–3616.

[9] D. Juric, G. Tryggvason, A front-tracking method for dendritic solidification, J. Comput. Phys. 123 (1996) 127–148.
[10] J. Fukai, T. Ozaki, H. Asami, O. Miyatake, Numerical simulation of liquid droplet solidification on substrates, J. Chem. Eng. Japan 33 (2000) 630–637.
[11] J.B. Collins, H. Levine, Diffuse interface model of diffusion-limited crystal growth, Phys. Rev. B 31 (1985) 6119–6122.
[12] Y.-T. Kim, N. Goldenfeld, J. Dantzig, Computation of dendritic microstructures using a level set method, Phys. Rev. E 62 (2000) 2471–2474.
[13] M. Ehrun, S.G. Advani, A BEM approach to model heat flow during crystallization, Int. J. Numer. Methods Eng. 35 (1992) 351–368.
[14] S. Osher, R. Fedkiw, Level set methods: an overview and some recent results, J. Comput. Phys. 169 (2001) 463–502.
[15] D.M. Anderson, G.B. McFadden, A.A. Wheeler, Diffuse-interface methods in fluid mechanics, Annu. Rev. Fluid Mech. 30 (1998) 139–165.
[16] L.C. Wrobel, A boundary element solution to Stefan's problem, in: Boundary Elements V, Springer, Berlin, 1983, p. 173.
[17] B. Merriman, J.K. Bence, S.J. Osher, Motion of multiple junctions: a level set approach, J. Comput. Phys. 112 (1994) 334–363.
[18] D. Jacqmin, Contact-line dynamics of a diffuse fluid interface, J. Fluid Mech. 402 (2000) 57–88.
[19] P.K. Kythe, An Introduction to Boundary Element Methods, CRC Press, Boca Raton, 1995.
[20] W.W. Schultz, M.G. Worster, D. Anderson, Solidifying sessile water droplets, EUROMECH Colloquium 408, Interactive Dynamics of Convection and Solidification, March 2000, Chamonix, France.
[21] M. Kelmanson, An integral equation method for the solution of singular slow flow problem, J. Comput. Phys. 51 (1983) 139–158.
[22] T.Y. Hou, J.S. Lowengrub, M.J. Shelley, Removing the stiffness from interfacial flow with surface tension, J. Comput. Phys. 114 (1994) 312–338.
[23] W. Press, S. Teukolsky, W. Vetterling, B. Flannery, Numerical Recipes, Cambridge University Press, Cambridge, 1992.